# Disruption of cerebellar microzonal organization in GluRδ2 (GluD2) knockout mouse

# GluRδ2（GluD2）ノックアウトマウスにおける 小脳微小帯域構造の異常

機能生物学専攻神経生理学分野

狩野方伸　教授

橋爪　幹

# TABLE OF CONTENTS

**ABSTRACT**

Cerebellar cortex has an elaborate rostrocaudal organization comprised of numerous microzones. Purkinje cells (PCs) in the same microzone show synchronous activity of complex spikes (CSs) evoked by excitatory inputs from climbing fibers (CFs) that arise from neurons in the inferior olive (IO). The synchronous CS activity is considered to depend on electrical coupling among IO neurons and anatomical organization of the olivocerebellar projection. I estimated how the CF-PC wiring contributes to synchronous CS activities by examining the glutamate receptor δ2 knockout (GluRδ2 KO) mice in which exuberant surplus CFs make ectopic innervations of PC dendrites. I performed *in vivo* two-photon calcium imaging for PC populations and examined dendritic calcium signals representing CF inputs. Neighboring PCs in GluRδ2 KO mice showed higher synchrony of calcium transients than those in wild-type mice. Moreover, the synchrony in GluRδ2 KO mice hardly declined with mediolateral separation between PCs up to ~200 μm, which was in marked contrast to the falloff of the synchrony at the same distance in wild-type mice. The enhanced synchrony was only partially affected by pharmacological blockade of gap junctional coupling. In contrast, transverse CF collaterals in GluRδ2 KO mice extended beyond the border of microzone and formed ectopic CF synapses on PC dendrites. These elongated CF collaterals

induced localized calcium transients in PC distal dendrites, which contributed to the

enhanced synchrony of calcium signals in GluRδ2 KO mice. These results strongly

suggest that proper formation of longitudinal olivocerebellar projection is essential for

spatiotemporal organization of CS activity in cerebellum.

**INTRODUCTION**

The cerebellum consists of several parasagittal zonal compartments elongated along rostrocaudal direction (designated A, B, C1–3 and D1–2). These compartments are based on the topography of the olivocerebellar projection system that constitutes one of the two major afferent systems to the cerebellum [1-4]. These cerebellar zones are thought to be involved in the control of different aspects of posture, movement and motor coordination [5, 6]. Moreover, several physiological studies have revealed that each cerebellar zone is composed of smaller functional units, called microzones [7-11]. Detailed morphological studies have revealed that axons of neurons in the inferior olive (IO) branch into about 7 climbing fibers (CFs) along rostrocaudal axis of the cerebellum, and each CF innervates a single Purkinje cell (PC) [1, 12, 13]. Experiments with a small injection of anterograde tracer into the IO have demonstrated that a small number of adjacent IO neurons project CFs within narrow longitudinal bands of about 200 μm width [1, 12], which correspond to physiologically identified microzones [7, 9]. Because of this anatomical organization and electrical coupling among adjacent IO neurons, CF inputs are synchronized among PCs within a microzone, and the synchrony rapidly falls off as the mediolateral separation between PCs increases [14-17].

A major hypothesis as to the function of the olivocerebellar system is that CFs

convey error signals to PCs between the intention and the result of movement [18]. Defects in the olivocerebellar system results in impairment of motor control and coordination [6, 18, 19]. It has been shown that several mutant mice that are impaired in developmental CF synapse elimination exhibit ataxia [20-25], suggesting that proper wiring of CFs to PCs is important for motor coordination. Among these examples, the mutant mouse deficient in ionotropic glutamate receptor $\delta2$ subtype (GluR$\delta2$) is best characterized by morphological, electrophysiological and behavioral studies. GluR$\delta2$ is richly expressed at dendritic spines of PCs that form synaptic contacts with terminals of parallel fibers (PFs) [26-28]. GluR$\delta2$ is essential for the formation and stabilization of PF-PC synapses by interacting with Cbln1 that binds to neurexin at PF terminals [29, 30]. Thus, the GluR$\delta2$ knockout (KO) mouse [21] has been shown to exhibit various defects in synaptic wiring and neuronal response: 1) the number of PF-PC synapse is reduced to nearly half of that of wild-type mouse, which results in emergence of numerous free spines in PC distal dendrites [31-33], 2) CFs extend distally along PC dendrites, take over spines from PFs and form ectopic synapses on PC distal dendrites [32]. 3) transverse collaterals of CFs that run perpendicularly to the plane of PC dendritic tree are markedly elongated and form ectopic synapses on distal dendrites of neighboring PCs along the mediolateral axis [34, 35], 4) stimulation of the aberrant CFs

in cerebellar slices induces atypical excitatory postsynaptic responses with slow rise time and small amplitudes in PCs which are associated with calcium transients localized to distal dendritic arbors [34, 36], and 5) PCs in GluRδ2 KO mice *in vivo* exhibit atypical "clustered firing (Cf)" [37], which is considered to be induced by ectopic CF inputs to PC distal dendrites. Thus, GluRδ2 KO mice provide an excellent model to study how altered CF to PC wiring affects population activity of PCs and functional microzonal organization *in vivo*.

In the present study, I employed *in vivo* two-photon calcium imaging [9, 14, 38] for PC populations and examined dendritic calcium signals representing CF inputs. I demonstrated that the degree of synchrony in CF inputs between neighbouring PCs was much higher in GluRδ2 KO mice than in wild-type mice. Moreover, the synchrony of CF inputs in GluRδ2 KO mice hardly declined with mediolateral separation between PCs, whereas the synchrony fell off over ~200 μm, which corresponded to the width of a microzone, in wild-type mice. I also showed that the enhanced synchrony in GluRδ2 KO mice was mainly ascribed to the aberrant CF to PC wiring, especially to elongated transverse CF collaterals, and also presumably to altered IO firing. Thus, proper formation of CF to PC wiring is a basis for functional microzonal organization in the cerebellum.

## MATERIALS AND METHODS

### Animals and Surgery

I used homozygous Grid2-Cre knock-in mice on pure C57BL/6 genetic background [39] as GluRδ2 knockout (GluRδ2 KO) mice. The GluRδ2 KO mice and their wild-type (WT) littermates were produced by mating heterozygous animal pairs. All experimental procedures were approved by Animal Experimental Committees of The University of Tokyo and Hokkaido University, and all animal experiments were performed according to the guidelines.

Male or female mice aged 1-3 months were anesthetized by intraperitoneal injection of ketamine (100 mg/kg) and xylazine (10 mg/kg). I confirmed the depth of anesthesia by monitoring the lack of whisker movements and pinch withdrawal reflex, and injected additional dose as needed. Body temperature was kept at 36 °C with a heating pad (FHC). The head of the animal was fixed by ear bars and the skull was exposed by removing skins, muscles and connective tissues on it. The occipital bone at the Crus IIa region (centered 4 mm lateral and 2 mm posterior to the occipital bone line) on the left cerebellar hemisphere was drilled to make a small hole (~2 mm in diameter). The dura matter was removed and the surface of the cerebellar cortex was cleaned with extracellular solution composed of (in mM) 150 NaCl, 2.5 KCl, 2 $CaCl_2$, 1 $MgCl_2$ and

10 HEPES (pH 7.4, adjusted with NaOH). Cortical surface was covered with 1.5 %
agarose dissolved in the extracellular solution, and a small coverslip was placed on half
of the cranial window, in order to reduce brain vibration caused by respiration and heart
beat.

**Dye injection and population calcium imaging**

Multi-cell bolus-loading of calcium indicator dye was performed as described [9, 14, 38,
40, 41]. Oregon Green 488 BAPTA-1 acetoxymethyl ester (OGB-1 AM, ~200 μM;
Invitrogen), was dissolved with 10 % w/v Pluronic F-127 (Invitrogen) in DMSO and
filled into a glass pipette (5-7 MΩ) together with the extracellular solution containing
Alexa 594 fluorescent dye (20 μM; Invitrogen). Dye ejection was performed in the
cerebellar molecular layer (50–60 μm from surface) at 5 psi for 3 minutes by using
Picospritzer (General Valve). Successful dye ejection was monitored by two-photon
imaging on Alexa channel. More than 30 minutes after dye ejection, I performed
calcium imaging in the molecular layer. To obtain calcium transients from populations
of PC dendrites, images were acquired at the resolution of $256 \times 64$ or $128 \times 128$ pixels
(sampling rate = ~8 Hz) for ~2 minutes. These image stacks were analyzed offline. For
detecting local calcium transients in bolus-loaded specimen, line-scan imaging

(sampling rate = 500 Hz) was performed on single PC dendrites of GluRδ2 KO mice.

### *In vivo* two-photon microscopy

*In vivo* calcium imaging was performed by using a two-photon microscope [42] controlled by Prairie view software (Prairie technologies), or a custom-built two-photon microscope (Sutter Instruments) controlled by ScanImage software [43]. The cerebellum was illuminated with a pulsed Ti:sapphire laser (810-840 nm in wavelength, 80 MHz repetition rate, 100 fsec pulse width; Spectra-Physics). Laser was focused through a 40× water-immersion objective lens (Olympus) onto the tissue. Average laser power was adjusted to be less than 20 mW at the specimen. Fluorescence signals of OGB-1 and Alexa 594 were divided into green and red channels respectively by a dichroic mirror and emission filters (Chroma), and were detected by a pair of photomultiplier tubes (Hamamatsu).

### Simultaneous dendritic calcium imaging and extracellular recording

A glass electrode (5-7 MΩ) filled with the extracellular solution containing Alexa 594 was inserted into the cerebellum and attached to a PC soma that had been loaded with

OGB-1 AM. About 10 minutes after the establishment of cell-attached configuration,

simultaneous extracellular unit recording and dendritic calcium imaging was performed.

Electrophysiological data were obtained by Multiclamp 700B (Molecular device) and

filtered at 10 kHz and digitized at 20 kHz using Digidata 1322A (Axon instruments)

controlled by Axograph X software (AxoGraph Scientific). Simple spikes (SSs), CSs

and clustered firing (Cf) [37] were distinguished by their characteristic waveforms. CS

showed a prominent spike followed by several spikelets with smaller amplitude. The

burst of 2-7 full-amplitude SS-like spikes occurred at >181 Hz (spike train with <5.5

msec of inter-spike interval) was defined as Cf according to the criterion in the previous

study [37]. After the recording session, negative current (<-20 nA) was injected into the

recorded cell to rupture the membrane and to stain it with Alexa 594, and a

morphological image stack for Alexa 594 was obtained to identify the dendrites of the

recorded cell among multiple OGB-1 positive PC dendrites in calcium imaging data.


**Drug application**

Carbenoxolone (120 mg/kg; Sigma), an inhibitor of gap junction, was dissolved in

saline (0.8 % w/v) and intraperitoneally injected to mouse in which OGB-1 AM had

been bolus-loaded. Then, calcium imaging was performed at every 20 minutes until 120

minutes after the drug application.

**Whole-cell recording and dendritic calcium imaging**

For *in vivo* whole-cell current-clamp recording, I used a potassium-based intracellular solution composed of (in mM): 133 potassium methanesulfonate, 7.4 KCl, 10 HEPES, 3 $Na_2ATP$, 0.3 $Na_2GTP$, 0.3 $MgCl_2$, 0.05 Alexa 594 and 0.2 OGB-1 (285 mmole/kg, pH 7.2 adjusted with KOH). According to shadowpatching method [44], PCs were visualized with negative contrast to obtain targeted recordings. A glass electrode (5-9 $M\Omega$) was brought to a PC soma under visual control and a brief suction was applied to form tight gigaohm seal. Cell membrane was then ruptured by short pulses of negative pressure to establish the whole-cell configuration. At least 30 minutes after break-in, line-scan calcium imaging (500Hz) on dendrite was performed at ~100 μm from the soma and the membrane potential was simultaneously recorded.

**Data analysis**

All image analysis was performed offline by using ImageJ software (http://rsb.info.nih.gov/ij/). Regions of interest (ROIs) corresponding to individual PC

dendrites were manually identified. Calcium transients were obtained from time-series image stack and expressed as $\Delta F/F = (F-F_0) / (F_0-F_b)$, where $F_0$ was baseline fluorescence without calcium transient and $F_b$ was background fluorescence. Mediolateral separation between PC dendrites was measured from a single high-resolution image of the recording field. The detection threshold for calcium transient was defined as 2 s.d. of $\Delta F/F$ for entire recording time. Cross-correlation coefficients were calculated by the formula below [45] using Igor pro software (Wavemetrics).

$$C_{ij(\tau)} = \frac{\sum_{t=0}^{T} X_{i(t)} X_{j(t+\tau)}}{\sqrt{\sum_{t=0}^{T} \{X_{i(t)}\}^2 \sum_{t=0}^{T} \{X_{j(t)}\}^2}}$$

where, $X_i$ and $X_j$ were calcium transient traces of $i$th and $j$th dendrites, $T$ was total recording time and $\tau$ was lag time between the 2 traces. $C_{ij}(0)$, cross-correlation coefficient at zero lag time, was defined as synchrony. Statistical significance of the data was examined by Mann-Whitney U test unless otherwise noted, and all tests were performed using Sigmastat 3.1 (Cranes Software International) or R (http://www.r-project.org/).

**Anterograde tracer labelling**

Mice at P56 were anesthetized by intraperitoneal injection of chloral hydrate (350 mg/kg) and head-clamped by a stereotaxic instrument (SR-5N; Narishige). A glass pipette filled with 2-3 μl of 10 % solution of dextran Alexa 594 (DA-594; Invitrogen) in PBS was inserted into the inferior olive by dorsal approach. The tracer was injected by air pressure at 20 psi with 5 sec intervals for 1 minute (Pneumatic Picopump; World Precision Instruments). After 4 days of survival, mice were anesthetized by intraperitoneal injection of pentobarbital (100 mg/kg) and transcardially perfused with 4 % paraformaldehyde in 0.1 M sodium phosphate buffer (pH 7.4). After excision from the skull, brains were further immersed overnight in the same fixative. Horizontal cerebellar sections with 50 μm thickness were prepared using a microslicer (VT1000S; Leica).

**Immunohistochemistry**

Horizontal cerebellar sections were obtained from 3 wild-type and 3 GluRδ2 KO mice. All immunohistochemical incubations were done at room temperature in a free-floating state. At first, cerebellar sections were incubated with 10 % normal donkey serum for 20 minutes. Then, a mixture of primary antibodies, including a guinea pig anti-vesicular

glutamate transporter 2 (VGluT2) antibody and a rabbit anti-aldolase C (aldC) antibody, was applied to slices overnight, followed by an incubation with Alexa 488- and Cy5-conjugated species-specific secondary antibodies (Invitrogen; Jackson ImmunoResearch) for 2 hours at a dilution of 1:200. Images of stained molecular layer were taken with a confocal laser scanning microscope (FV1000; Olympus) equipped with digital camera (DP70; Olympus), and analyzed with MetaMorph software (Molecular Devices).

**RESULTS**

**Highly synchronous spontaneous calcium transients in neighboring PCs in GluRδ2 KO mice**

In rat and mouse, spontaneous calcium transients in PC dendrites *in vivo* have been shown to be attributed to CSs evoked by CF input [9, 14, 38, 40, 46, 47]. To compare the spatial pattern of CS firing in PCs of GluRδ2 KO mice with that of wild-type mice, OGB-1 AM was bolus-loaded into the molecular layer of the cerebellar cortex [14, 40, 46]. About 30 minutes after dye-loading, OGB-1 was penetrated into various cell types, including PCs, interneurons and Bergmann glia. In the molecular layer, dendrites of PCs extending along rostrocaudal axis were clearly observed (Fig. 1A). Spontaneous fluorescence changes induced by calcium influx were observed in individual PC dendrites. In wild-type mice, calcium transients occurred at various timing in each dendrite with occasional highly synchronized transients between neighboring dendrites (Fig. 1B, upper), which is consistent with the previous results [9, 14, 38, 40, 46]. In contrast, almost all calcium transients in GluRδ2 KO mice occurred at the same time in all of the dendrites observed (Fig. 1B, lower). Cross-correlation coefficient was calculated to quantify synchronous activity between neighboring PCs (Fig. 1C), and the relationship between the synchrony and the distance between the dendrites in mediolateral direction was analyzed for all dendritic pairs in the field of view (Fig. 1D).

As previously reported, synchrony in wild-type mice fell off as the mediolateral separation between PC dendrites increased [9, 14]. In marked contrast, the synchrony in GluRδ2 KO mice was almost constant at all the mediolateral separations examined. On average, the synchrony in GluRδ2 KO mice was significantly higher than that in wild-type mice at all the distances of mediolateral separation (1064 dendrite pairs in 26 GluRδ2 KO mice and 1009 pairs in 33 wild-type mice, $p < 0.001$ in Two-way ANOVA) (Fig. 2A), and the rate of decline in synchrony was smaller in GluRδ2 KO mice than in wild-type mice (Fig. 2B). These results indicate that the synchrony of spontaneous CSs among neighboring PCs is greatly enhanced in GluRδ2 KO mice, and the spatial range of synchrony is extended in mediolateral direction.
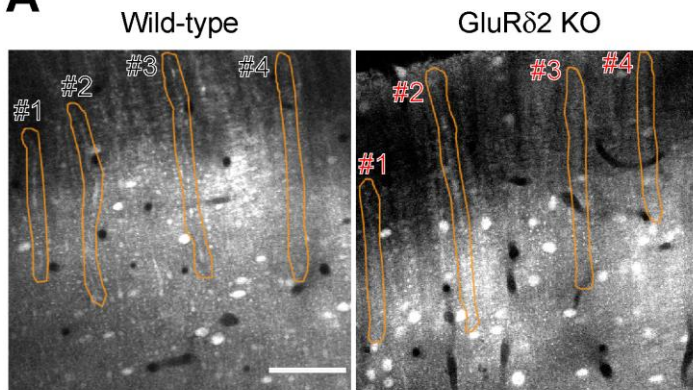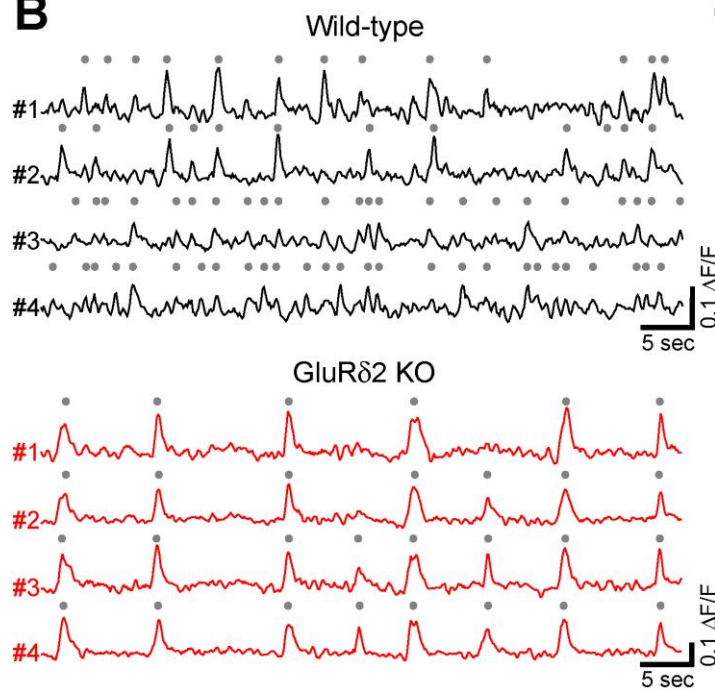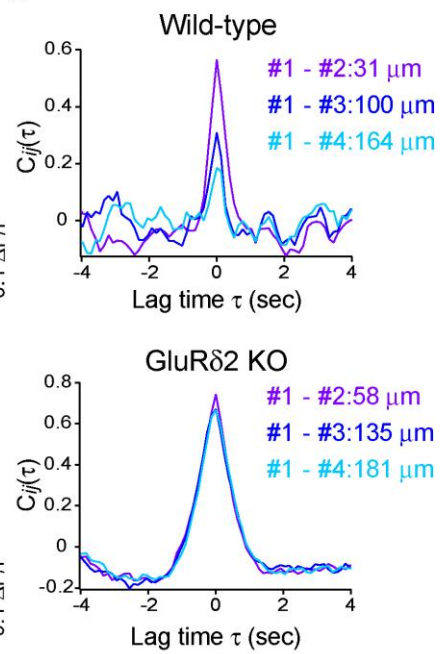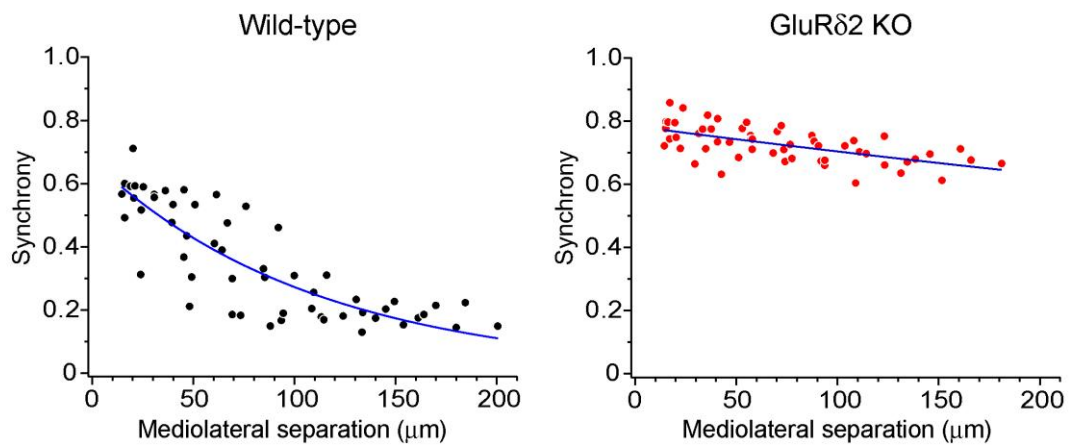
**A** Wild-type    GluRδ2 KO

**B** Wild-type

GluRδ2 KO

**C** Wild-type

$C_{ij}(\tau)$

#1 - #2:31 μm
#1 - #3:100 μm
#1 - #4:164 μm

Lag time τ (sec)

GluRδ2 KO

$C_{ij}(\tau)$

#1 - #2:58 μm
#1 - #3:135 μm
#1 - #4:181 μm

Lag time τ (sec)

**D** Wild-type    GluRδ2 KO

Synchrony

Mediolateral separation (μm)

**Figure 1**

Synchrony of spontaneous calcium transients in wild-type and GluRδ2 KO mice.

(A) Fluorescent images showing the molecular layer of the cerebellar cortex labeled with OGB-1 AM in wild-type and GluRδ2 KO mice. PC dendrites are seen as gray bands that extend along the rostrocaudal axis and aligned perpendicular to the mediolateral axis. Spontaneous calcium transients were obtained by monitoring fluorescent changes of the specified regions of interest (ROIs; orange). Scale bar, 50 μm. (B) Representative traces of calcium transient from 4 dendrites (#1-#4) that correspond to the ROIs in A. Gray dots indicate detected calcium transients from baseline noise. (C) Cross-correlation coefficients for the traces in B were calculated between #1 and the other dendrites, and the mediolateral separations between the dendrites were measured. Synchrony (i.e., the cross-correlation at zero lag time, see Materials & Methods) in wild-type mice was the highest at the nearest neighboring pair, and gradually decreased as the mediolateral separation increased. In marked contrast, synchrony in GluRδ2 KO mice was almost constant regardless of the mediolateral separation. (D) Summary graphs for the synchrony between all dendrite pairs plotted against mediolateral separations from the wild-type and GluRδ2 KO mice shown in A (55 dendrite pairs). Blue curves indicate the exponential fit to the data.
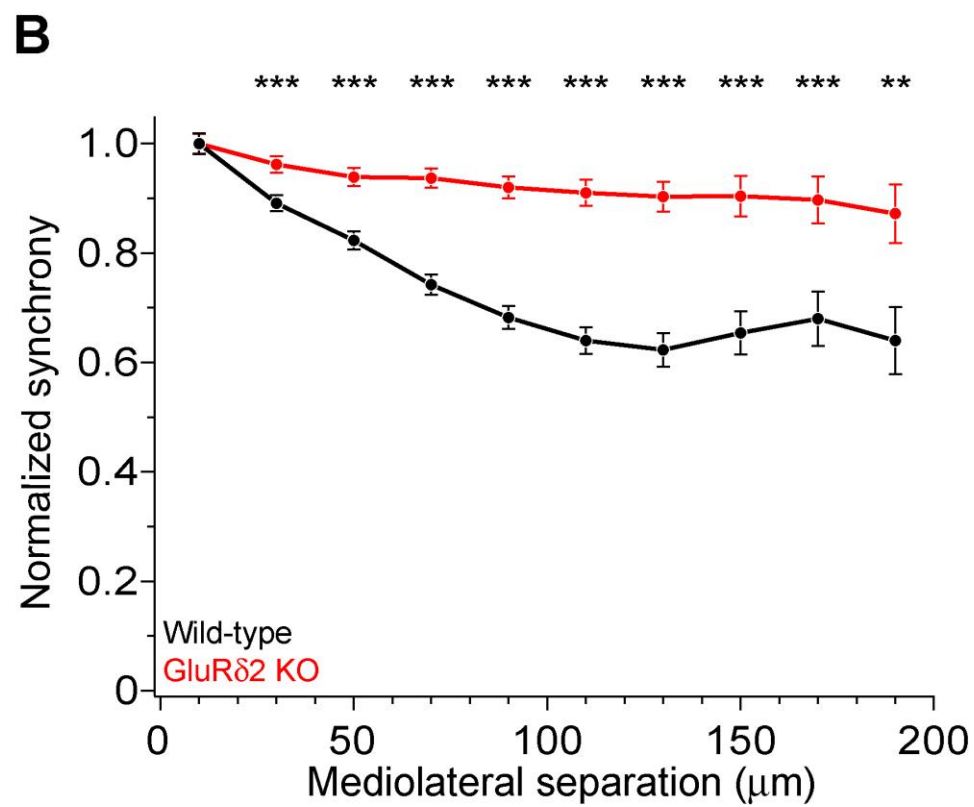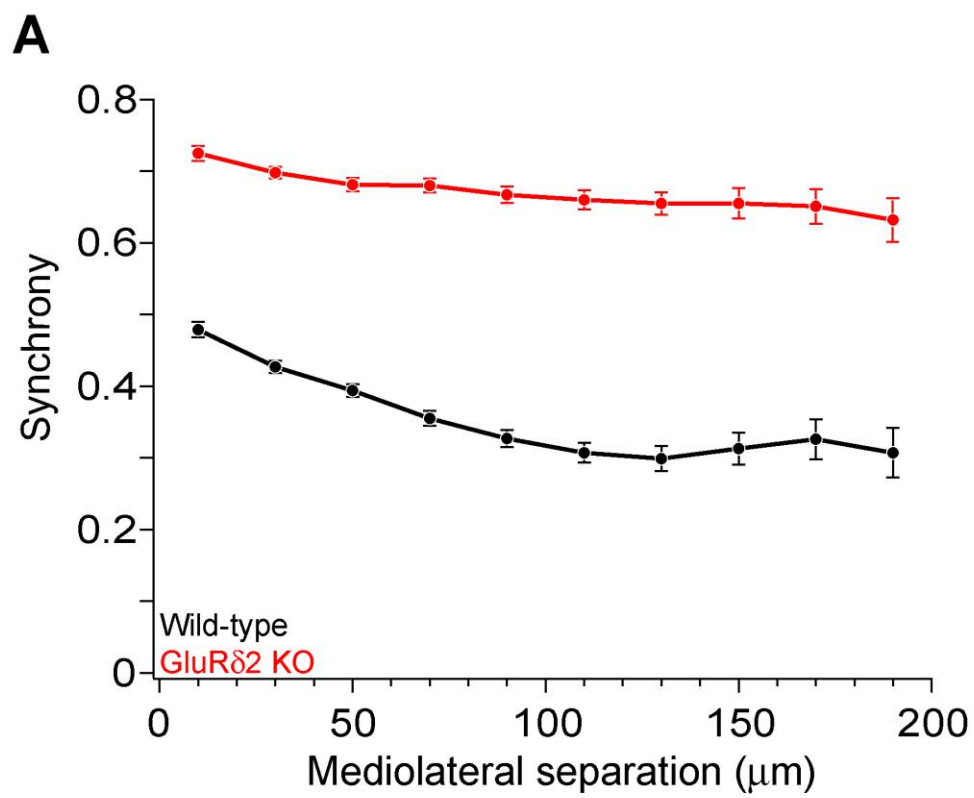
**Figure 2**

Enhanced synchrony between dendrite pairs of GluRδ2 KO mice at all distances of mediolateral separation.

(A) Summary graph showing pooled data of synchrony plotted against mediolateral separation for 1009 dendrite pairs obtained from 33 wild-type mice (black symbols) and for 1064 dendrite pairs from 26 GluRδ2 KO mice (red symbols). Each data point represents the average of synchrony and error bars indicate SEM. There was significant difference between the 2 genotypes (***$p < 0.001$ in Two-way ANOVA). (B) All values of synchrony were normalized by the mean value of the nearest dendrite pairs within the mediolateral separation of 20 μm. Difference between wild-type and GluRδ2 KO mice were tested at all separations by Two-way ANOVA and Turkey test. As a result, there was significant difference between the 2 genotypes in all but the nearest point (**$p < 0.01$, ***$p < 0.001$), indicating that the degree of decline in synchrony along the mediolateral direction is much smaller in GluRδ2 KO mice than that in wild-type mice.

**Relationship between calcium transient and CF input in GluRδ2 KO mice**

In addition to the enhancement of the synchrony between calcium transients of neighboring PCs, I found that the frequency of calcium transient in GluRδ2 KO mice was lower than that in wild-type mice ($0.15 \pm 0.01$ Hz and $0.29 \pm 0.02$ Hz, respectively; 11 mice each, $p < 0.001$)(Fig. 1B), and the half-width of transients was larger in GluRδ2 KO mice than in wild-type mice ($0.710 \pm 0.01$ sec and $0.517 \pm 0.01$ sec, respectively; 5 mice each, $p < 0.001$), suggesting that the temporal pattern of CS firing has changed in GluRδ2 KO mice. Therefore, simultaneous dendritic calcium imaging and extracellular recording were performed on single PCs to clarify the electrophysiological correlates of calcium transients (Fig. 3A). Cell-attached recordings in both wild-type and GluRδ2 KO mice showed ongoing simple spikes (SSs) and sporadic CSs (Fig. 3B). The mean firing rates of SS ($22.12 \pm 5.39$ Hz in wild-type and $17.19 \pm 2.33$ Hz in GluRδ2 KO mice) and CS ($0.32 \pm 0.04$ Hz in wild-type and $0.40 \pm 0.03$ Hz in GluRδ2 KO mice) were not significantly different between the 2 genotypes (13 mice each; $p > 0.09$ and $p > 0.1$, respectively). Although calcium transients were induced by CS in both genotypes (Fig. 3C, 3D), each calcium transient in GluRδ2 KO mice tended to be associated with multiple successive CSs. The fraction of calcium transients induced by multiple CSs was significantly higher in GluRδ2 KO mice than in wild-type mice (Fig. 3E, $p < 0.001$

21

in $\chi^2$ test). Besides, the histogram of inter-CS interval clearly showed that CSs in GluR$\delta$2 KO mice were induced in rapid succession with short interval (Fig. 3F). These results indicate that the lower frequency and longer duration of calcium transients in GluR$\delta$2 KO mice were attributed to the altered CS firing pattern.

Atypical responses, termed "clustered firing" (Cf) [37], were observed only in GluR$\delta$2 KO mice at similar frequency to CS firing rate ($0.39 \pm 0.09$ Hz in 11 mice; $p > 0.1$; see Materials and Methods for the definition of Cf). Cf was thought to be induced by aberrant CF input [37]. Cfs showed similar or even shorter inter-Cf intervals than CS (Fig. 3F). Moreover, most Cfs occurred temporally close to CS (Fig. 3C, 3G). These results suggest that the firing pattern of IO neurons is altered in GluR$\delta$2 KO mice such that bursts of action potentials frequently occur in PCs.
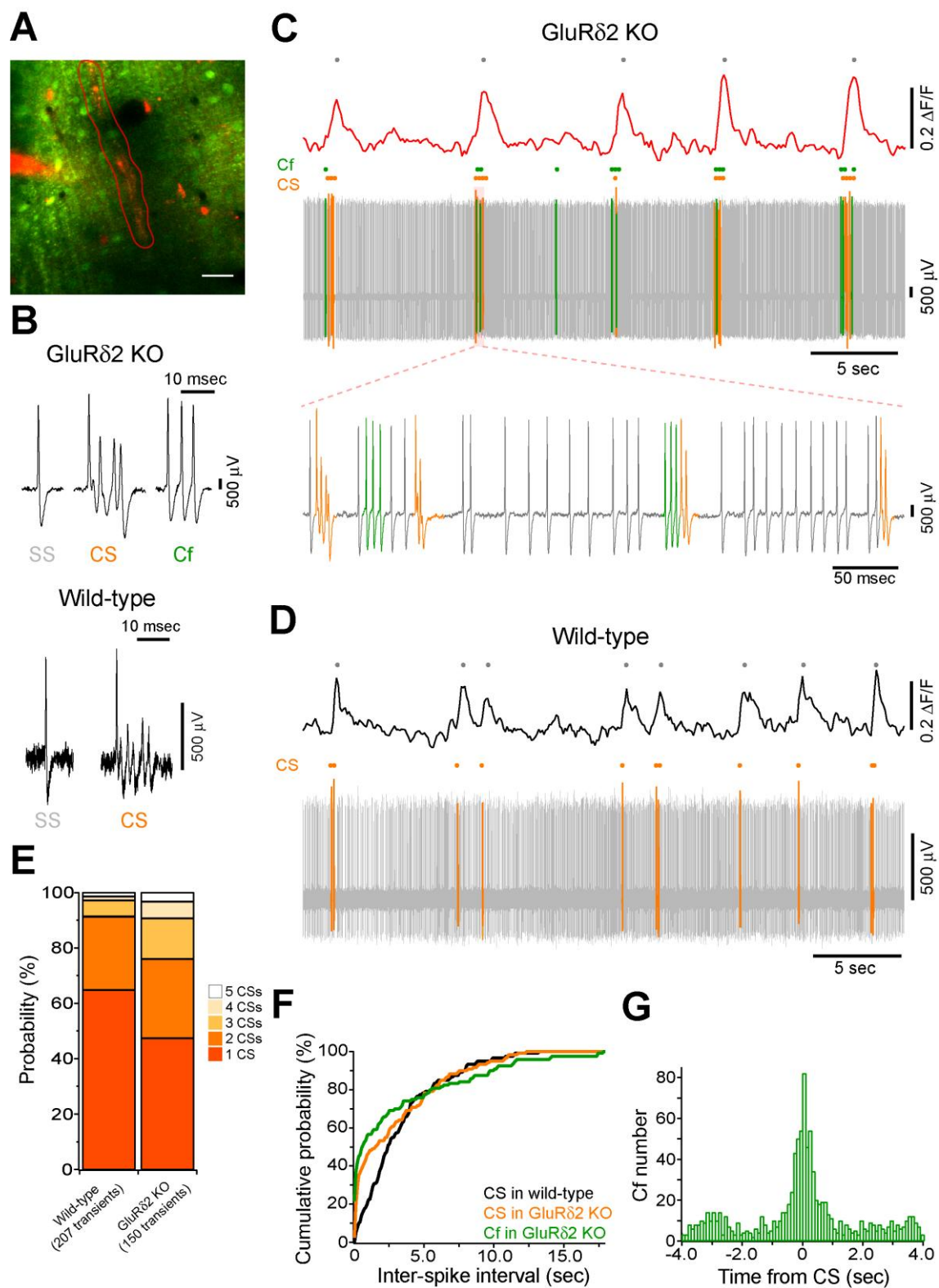
**Figure 3**

Altered CF activity patterns in GluRδ2 KO mice.

(A) Representative image showing the molecular layer that was loaded with OGB-1 AM in a GluRδ2 KO mouse. Simultaneous cell-attached recording and dendritic calcium imaging from single PCs were performed. After the recording, Alexa 594 was injected through the patch pipette to the PC from which cell-attached recording was conducted. Spontaneous calcium transients were obtained from the ROI enclosed by red line. Scale bar, 20 μm. (B) Sample traces for simple spike (SS), complex spike (CS) and clustered firing (Cf) under cell-attached recordings from GluRδ2 KO (upper panel) and wild-type (lower panel) mice. Cf was not observed in wild-type mice. (C) Simultaneous recording of PC firing and dendritic calcium transients in the PC shown in A. SS, CS and Cf are indicated in gray, orange and green, respectively. Note that calcium transients are elicited only when CS occurs, or when CS and Cf fire in cluster. The bottom trace shows clustered CS and Cf in an expanded timescale. In this period, a single calcium transient included multiple CSs and Cfs that fired in temporal proximity. (D) Simultaneous recording of PC firing and dendritic calcium transients in a wild-type PC. Note that all the calcium transients are associated with CSs. (E) Bar chart showing the proportion of calcium transient induced by 1 to 5 CSs. The fraction of each component was significantly different between wild-type and GluRδ2 KO mice (4 mice for each genotype; ***p < 0.001 in $\chi^2$ test). (F) Cumulative probability plot of inter-spike intervals for CS and Cf. Each curve is composed of 120 intervals obtained from 6 mice for each genotype. Curves for CS and Cf in GluRδ2 KO mice were significantly different from the curve for CS in wild-type mice (***p < 0.001 in KS-test). Moreover, there was a significant difference between the curve for CS and that for Cf in GluRδ2 KO mice (**p = 0.004 in KS-test). Bin width, 100 msec. (G) Cross-correlogram of Cf against CS was constructed using the data from 8 GluRδ2 KO mice. Note that a prominent peak is present at 0 second. Bin width, 25 msec.

**The effect of gap junctional coupling on enhanced synchrony of CS activity in GluRδ2 KO mice**

According to previous reports, altered modulatory inputs in the IO by pharmacological manipulation causes change in rhythmicity and synchrony of CS firing [8, 45, 48]. To examine whether the change in electrical coupling among IO neurons made significant contribution to the enhanced synchrony of CS firing in GluRδ2 KO mice, carbenoxolone, a non-selective blocker of connexin, was intraperitoneally injected during calcium imaging experiments. About 1 hour after drug application, synchronized calcium transients were reduced in both wild-type and GluRδ2 KO mice (Figure 4A, 4B). As a result, the average synchrony significantly decreased (from 0.48±0.04 to 0.34±0.02 in 8 wild-type, p = 0.002 by paired t-test; from 0.73±0.03 to 0.55±0.04 in 5 GluRδ2 KO mice, p = 0.003). The degrees of reduction in the synchrony by carbenoxolone injection were not significantly different between the 2 genotypes (0.14±0.03 in wild-type and 0.18±0.03 in GluRδ2 KO mice; p > 0.1). Therefore, the values of synchrony at all the distances of mediolateral separation in GluRδ2 KO mice were still larger than those in wild-type mice even though electrical couplings in IO neurons were inhibited (Fig. 4B; p < 0.001 by Two-way ANOVA). When the values were normalized to those within 20 μm separation, the rate of decline in the synchrony

along mediolateral axis remained much smaller in GluRδ2 KO mice than in wild-type

mice after carbenoxolone application (Fig. 4C). While carbenoxolone enhanced the rate

of decline in the synchrony along mediolateral axis to some extent in wild-type mice, it

had much smaller effect in GluRδ2 KO mice (Fig. 4D). These results indicate that the

enhancement of synchrony along mediolateral direction is likely to be attributable

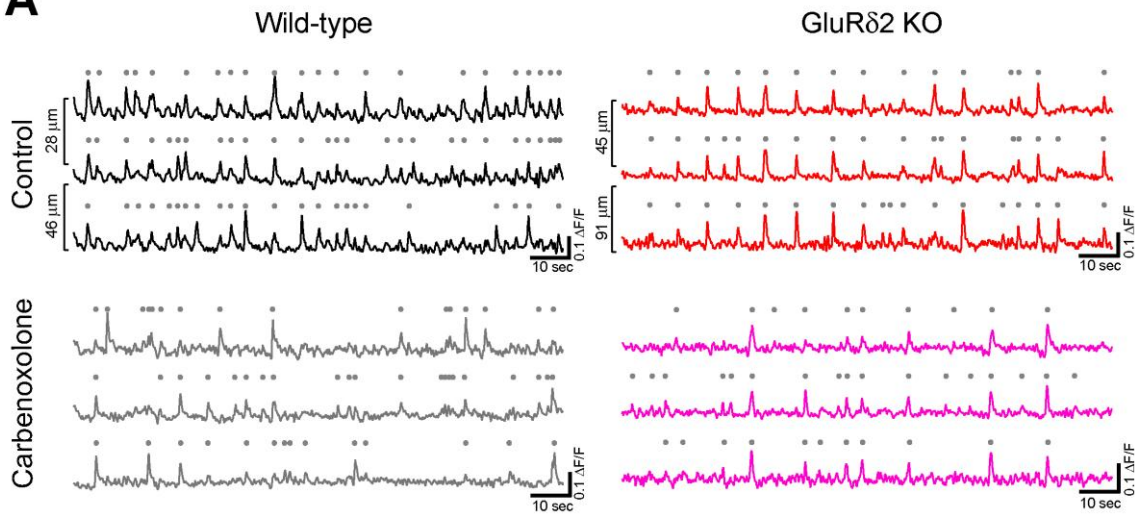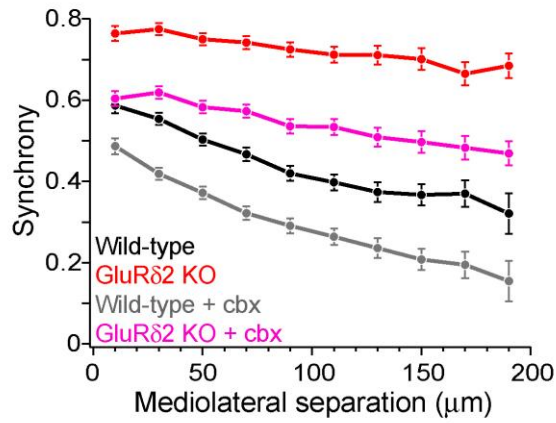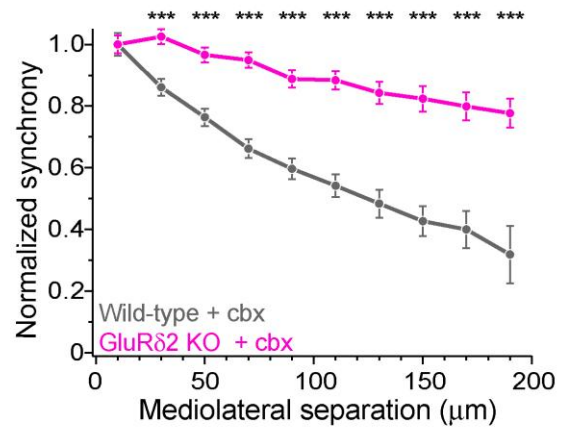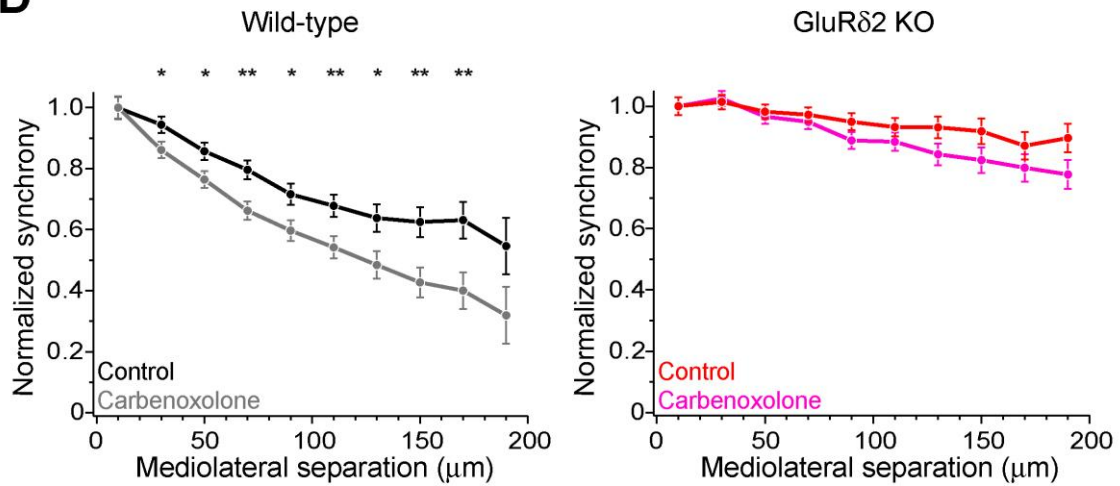largely to mechanisms other than gap junctional coupling in IO neurons.

**Figure 4**

Carbenoxolone reduced the synchrony but little altered the degree of decline along mediolateral axis in GluRδ2 KO mice.

(A) 3 representative traces of calcium transient from neighboring PC dendrites before (control) and ~1 hour after carbenoxolone injection (carbenoxolone), obtained from wild-type (left) and GluRδ2 KO (right) mice. Distances of mediolateral separation between dendrites are indicated on the left of the traces. In both genotypes, synchronous calcium transients appeared to be decreased by carbenoxolone. (B) Summary graph showing pooled data of synchrony for 318 dendrite pairs obtained from 8 wild-type mice and for 267 dendrite pairs from 5 GluRδ2 KO mice. Carbenoxolone (cbx) injection reduced mean values of synchrony in both genotypes. It should be noted that the difference between the genotypes was highly significant after carbenoxolone injection (wild-type + cbx (gray) vs GluRδ2 KO + cbx (magenda), ***$p < 0.001$ in two-way ANOVA), as was before drug application (wild-type (black) vs GluRδ2 KO (red), ***$p < 0.001$ in two-way ANOVA). (C) Normalized synchrony curves of wild-type and GluRδ2 KO mice after carbenoxolone injection. The rate of decline in GluRδ2 KO mice was significantly smaller than that in wild-type mice. (D) Normalized synchrony curves before and after carbenoxolone injection are plotted for wild-type (left graph) and GluRδ2 KO (right graph) mice to evaluate the effect of carbenoxolone on the rate of decline. In wild-type mice, synchrony was significantly decreased by corbenoxolone at all but the nearest and the farthest points of separation, whereas in GluRδ2 KO mice, significant differences were not detected at all separation points. All statistical tests were performed using Two-way ANOVA and Turkey test (*$p < 0.05$, **$p < 0.01$, ***$p < 0.001$).

**Multi-zonal projection of transverse branches from ascending CF in GluRδ2 KO mice**

I hypothesized that the enhanced mediolateral synchrony in GluRδ2 KO mice was due to disorganized olivocerebellar projection by the persistent multiple CF innervation [21, 32, 34, 36]. Immunohistochemical labeling of CF terminals combined with tracer injection into the IO has revealed that dendrites of PCs in GluRδ2 KO mice make contact with glutamatergic terminals from ascending CFs as well as from transverse collaterals of neighboring ascending CFs [32, 34]. Thus, these aberrant transverse branches were assumed to contribute to the enhanced mediolateral synchrony beyond the proper range of microzone in GluRδ2 KO mice. To elucidate whether CFs projecting to a microzone could extend their transverse branches to neighboring microzones in GluRδ2 KO mice, I examined the relationship between the extension of CF transverse branches and the expression pattern of aldolase C (aldC) in PCs. AldC is expressed in PCs aligned in longitudinal stripes [49-51], and the tight link between aldC compartments and CF projections [12, 52-54] and CS synchrony [55] have shown.

A small amount of dextran Alexa 594 (DA594) was injected into a certain subnucleus of the IO in order to visualize the trajectories of subsets of CFs and their innervation patterns. After 4 days of survival, mice were sacrificed, brains were

removed and cerebellar sections were prepared. The sections were immunostained for

aldC, type 2 vesicular glutamate transporter (VGluT2, a CF terminal marker) and

DA594. In wild-type mice, ascending CFs had a few short transverse branches (Figure

5A2, 5B2) that had no detectable VGluT2-positive puncta (Figure 5A1, 5B1). These

short processes (20.9±1.2 μm; n = 188) originated from an aldC-negative zone and did

not reach the neighboring aldC-positive zone (Figure 5A, 5B), and vice versa. By

contrast, much longer transverse branches (46.9±3.0 μm; n = 135, p < 0.001) containing

many VGluT2-positive puncta were observed in GluRδ2 KO mice (Figure 5C–F). These

branches bifurcated from ascending CFs located in an aldC-positive (Figure 5C, 5D) or

-negative (Figure 5E, 5F) zone, and elongated toward neighboring zones. Furthermore,

they made synaptic connections with multiple PCs aligned in the mediolateral axis

beyond the border of aldC compartments (Figure 5D, 5F). Notably, 28.1 % (38/135) of

total branches observed in the present study had numerous excitatory terminals to broad

region of PC dendrites in the neighboring zones (Fig. 5F; red and yellow arrowheads).

These morphological data strongly suggest that PCs within a certain microzone receive

inputs from ascending CFs in that microzone and from CF transverse collaterals
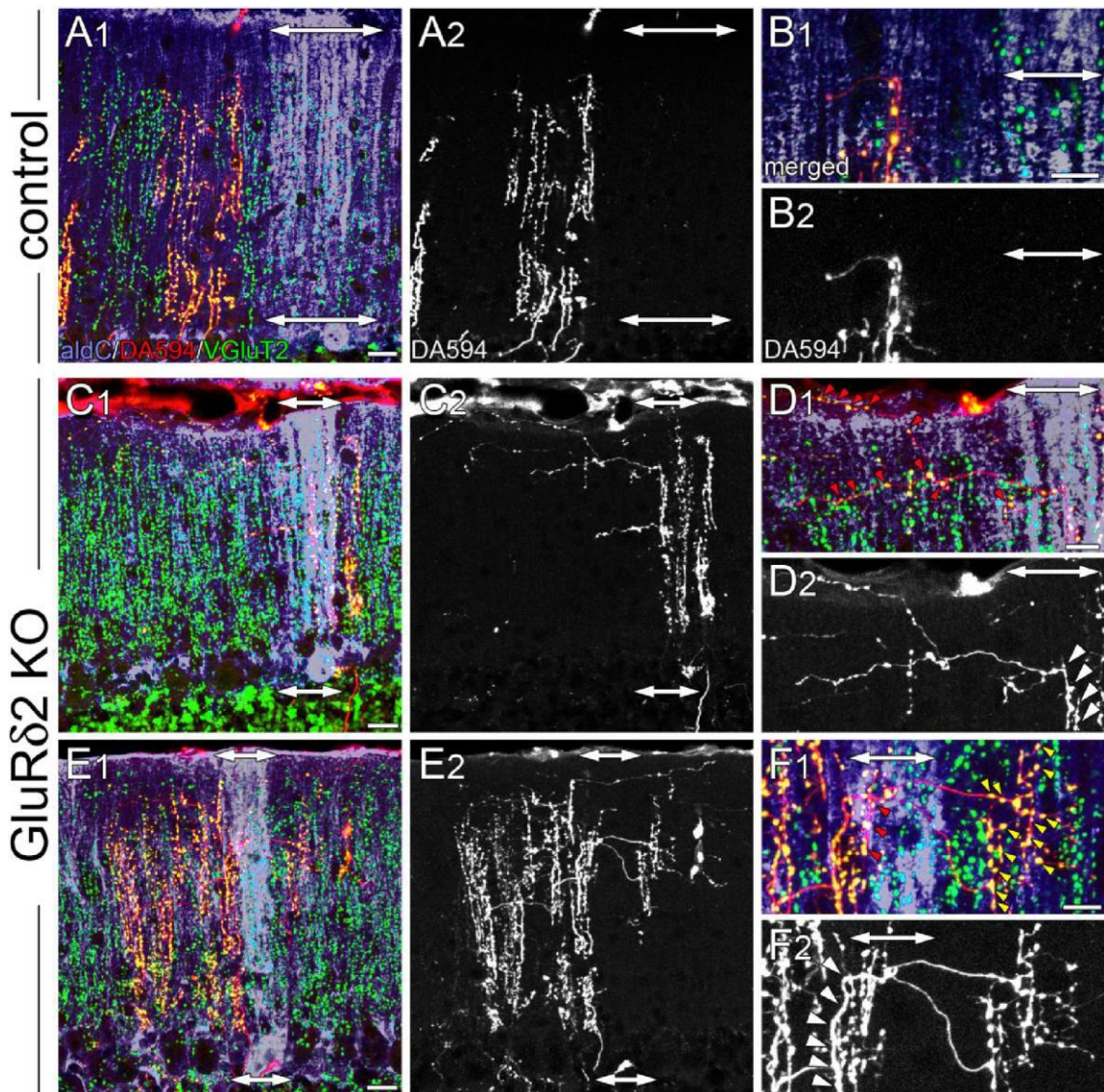
originating in neighboring microzones in GluRδ2 KO mice.

**Figure 5**

Ectopic CF innervations beyond the zones in GluRδ2 KO mice.

(A) Photomicrographs of a horizontal section of cerebellar cortex from a wild-type mouse. In A1, aldC (purple) and VGluT2 (green) positive structures are present besides CFs labeled with DA594 (red). Double-headed arrows indicate the region in which aldC-positive PCs are localized. In this case, the tracer was taken up by CFs projecting to aldC-negative zone. A2 is the same section as A1 but shows DA594-labelled CFs only. (B) Magnified pictures of the outer molecular layer near the pial surface in A1 and A2. There are short transverse CF collaterals that lack VGluT2-positive puncta and do not reach the adjacent aldC-positive zone. (C) Photomicrographs of a horizontal section of cerebellar cortex from a GluRδ2 KO mouse. In this case, transverse CF collaterals

bifurcate from ascending CFs that project to aldC-positive PCs. Note that transverse CF collaterals extend toward the adjacent aldC-negative zone. (D) Magnified pictures of the outer molecular layer near the pial surface in C1 and C2. Red arrowheads in D1 indicate VGluT2-positive glutamatergic terminals of transverse CF collaterals that form synaptic contacts onto multiple PCs. White arrowheads in D2 indicate the origins of transverse CF collaterals. (E) Photomicrographs of a horizontal section of cerebellar cortex in another GluRδ2 KO mouse. In this case, transverse CF collaterals bifurcate from ascending CFs that innervate aldC-negative PCs and extend toward the adjacent aldC-negative zone beyond the aldC-positive zone. (F) Magnified pictures of the outer molecular layer near the pial surface in E1 and E2. Red and yellow arrowheads in F1 indicate VGluT2-positive glutamatergic terminals of transverse CF collaterals that form numerous synaptic contacts onto aldC-positive and aldC-negative PCs, respectively. White arrowheads in F2 indicate the origins of transverse CF collaterals. Scale bar, 20 μm in A, C and E; 10 μm in B, D and F

32

**Calcium transients in distal dendrites induced by aberrant CF inputs in GluRδ2 KO mice**

To examine whether ectopic CF branches, including transverse branches can induce detectable calcium transient *in vivo*, simultaneous somatic whole-cell recordings and calcium imaging at distal dendrite were performed on single PCs in GluRδ2 KO mice (Fig. 6A). SS, CS and Cf were detected in current-clamp recordings (Fig. 6B). High-speed line-scan imaging (2 msec/line) was performed to detect individual calcium transients, because half of the CSs and Cfs occurred with subsecond inter-spike interval (Fig. 3F). CSs induced calcium transients over the entire dendritic arbor (Fig. 6C1; Fig. 6C2, orange traces and columns), which was the same as in wild-type mice and in rats [47]. By contrast, Cfs induced calcium transients only at a restricted region of distal dendrites (Fig. 6C). As exemplified in Fig. 6C, Cf-evoked transients were consistently observed only in the lower dendritic region (Fig. 6C1; Fig. 6C2 left panel, green trace and column) and virtually no calcium signals were detected in the upper dendritic region (Fig. 6C1; Fig. 6C2 right panel, green trace and column). This result is very similar to that obtained in cerebellar slice preparations from GluRδ2 KO mice [36] in which stimulation of surplus weak CFs induced calcium transients restricted to small regions of distal dendritic arbors of PCs. It should be noted that, although Cf-evoked

calcium transients were spatially localized, no significant difference was found between the amplitudes of calcium transients evoked by Cf and those by CS in the same dendritic regions (Fig. 6C2, left panel). Importantly, Cfs and localized calcium transients were not detected in wild-type mice (11 mice).

I also found that localized calcium transients could be detected in PC dendrites of GluRδ2 KO mice that were filled with OGB-1 AM by bolus-loading method (Fig. 6D). In the case shown in Fig. 6D1 and upper panel of Fig. 6D2, a calcium transient that was detected in both the upper and lower dendritic regions (Fig. 6D1, red and blue traces; Fig. 6D2 upper panel, orange traces) was followed by another calcium transient that was confined to the lower dendritic region (Fig. 6D1, blue trace; Fig. 6D2 upper panel, green traces). The summary data demonstrated that global and localized calcium transients were present in PC dendrites of GluRδ2 KO mice (Fig. 6D2 lower panel). The global and localized calcium transients of PCs in GluRδ2 KO mice by bolus-loading of OGB-1 AM (Fig. 6D) were very similar to CS-evoked and Cf-evoked calcium transients, respectively, in whole-cell recorded PCs in GluRδ2 KO mice (Fig. 6C). Since aberrant CF inputs to PCs in GluRδ2 KO mice are thought to induce Cfs in intact cerebellum [37] and local calcium transients in cerebellar slices [36], these results indicate that the localized calcium transients were caused, at least in part, by aberrant CF inputs from

transverse branches. The amplitudes of these localized calcium transients were comparable to those of the global calcium transients (Fig. 6C2 and 6D2). Therefore, the localized calcium transients elicited by CF transverse collaterals are likely to contribute to the enhanced synchrony of PC activity along the mediolateral axis.

**A**

Pia

Molecular layer

Purkinje cell layer

**B**

10 msec

20 mV

SS    CS    Cf

**C1**

29 μm

36 μm

0.2 ΔF/F

20 mV

-47 mV

200 msec

**C2**

0.1 ΔF/F

50 msec

0.1 ΔF/F

50 msec

Detected ROI

Undetected ROI

*

ΔF/F

CS    Cf

ΔF/F

CS    Cf

**D1**

31 μm

27 μm

0.1 ΔF/F

200 msec

**D2**

0.1 ΔF/F

50 msec

0.1 ΔF/F

50 msec

Detected ROI

Undetected ROI
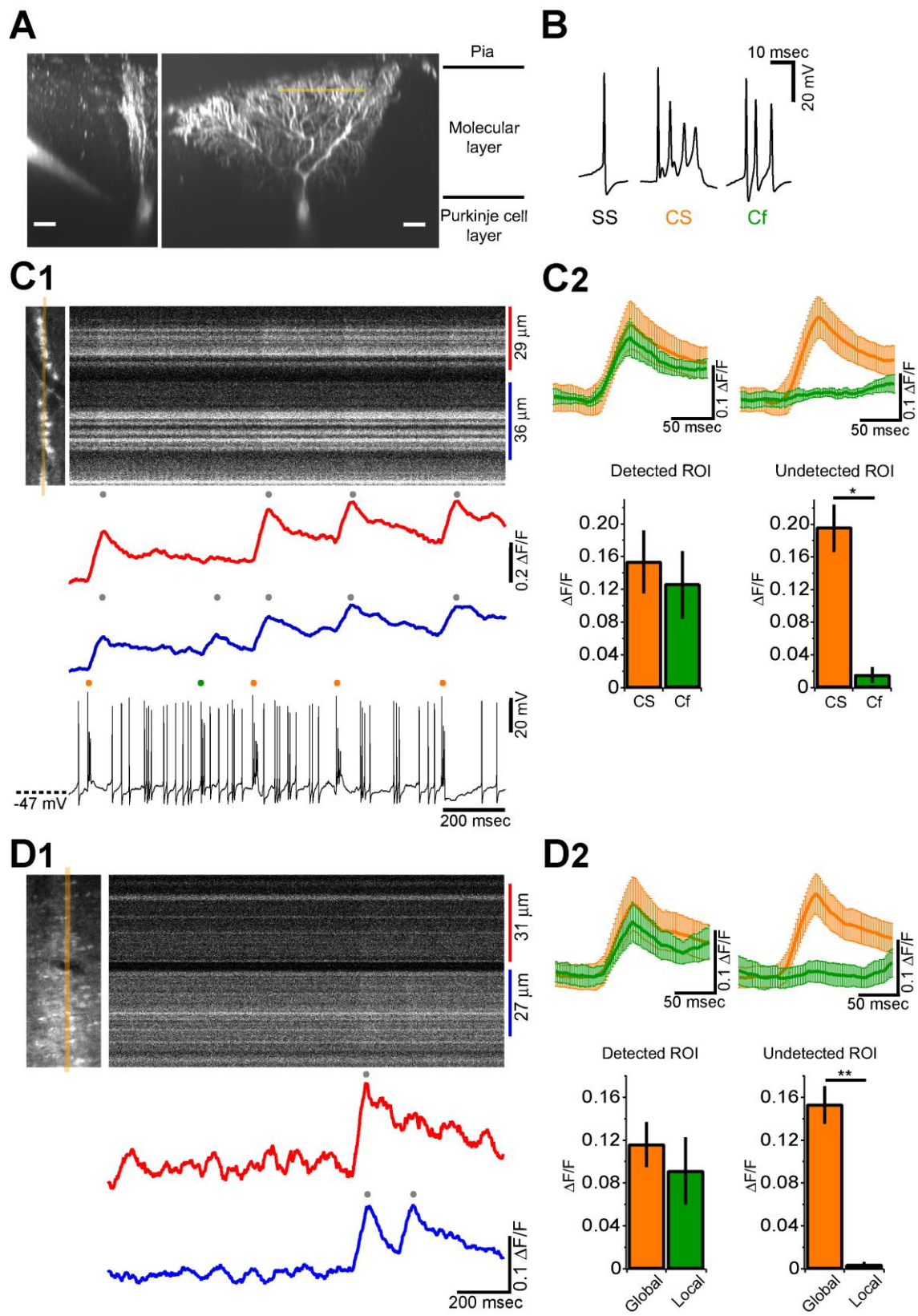
**

ΔF/F

Global    Local

ΔF/F

Global    Local

**Figure 6**

Local calcium transient induced by Cf in GluRδ2 KO mice.

(A) Fluorescent images showing a whole-cell patch-clamped PC of a GluRδ2 KO mouse in transverse (left) and sagittal (right) views that were taken more than 30 minutes after OGB-1 and Alexa 594 were filled through the patch pipette. Line-scan calcium imaging was performed at distal dendrite (~100 μm from the soma) indicated by orange line. Scale bar, 20 μm. (B) Sample traces of simple spike (SS), complex spike (CS) and clustered firing (Cf) under current-clamp recording from a GluRδ2 KO mouse. (C1) Simultaneous whole-cell recording and line-scan calcium imaging was obtained from the PC shown in A. Left image indicates the location of line-scan (orange line). ROIs were determined so that local calcium transients could be maximally recorded. The blue trace was obtained from the lower ROI in which local calcium transient was recorded, and the red trace was obtained from the upper ROI in which no local calcium transients were detected. The onset of local calcium transient coincided with the time when Cf occurred. (C2) (upper panels) Average traces of calcium transients induced by CS (orange trace) and by Cf (green trace) in the ROI from which Cf-evoked local calcium transients were detected (Detected ROI) and in the other ROI of the same PC in which Cf-evoked local calcium transients were absent (Undetected ROI). CS- or Cf-evoked calcium transients are shown as mean ± S.E.M from 4 GluRδ2 KO mice. Note that the magnitude and time course of Cf-evoked calcium transient in the detected ROI was comparable to those of CS-evoked calcium transient. (lower panel) Bar graphs show the magnitudes of calcium transients in the detected ROI (left) and undetected ROI (right). There was no significant difference in magnitude between CS-evoked and Cf-evoked calcium transients in the detected ROI (left, $p > 0.1$). By contrast, there was no detectable fluorescent change in the undetected ROI when Cf occurred (right; $*p = 0.03$). (D1) Line-scan imaging on a PC distal dendrite from a GluRδ2 KO mouse that was stained by bolus-loading of OGB-1 AM. Left picture indicate the location for line-scan (orange line). A local calcium transient was detected in the lower ROI (blue trace) but was absent in the upper ROI (red trace). (D2) Average traces of calcium transients (upper panels, from 5 GluRδ2 KO mice) and bar graphs showing the magnitudes of global and local calcium transients (lower panels) for the ROI from which local calcium transients were recorded (Detected ROI) and for the ROI in which local calcium transients were absent (Undetected ROI). Data are illustrated similarly to C2. There was no significant difference in magnitude between global and local calcium transients in the detected ROI. There was no detectable fluorescent change in the undetected ROI (right; $**p = 0.008$) at the time when local calcium transients occurred in the detected ROI.

**DISCUSSION**

In the present study, I demonstrated that PCs within a given microzone in GluRδ2 KO mice showed higher synchrony of CF activities than in wild-type mice, and the synchrony remained high even when the mediolateral separation increased. The enhancement of synchrony in mediolateral direction was ascribed to the local calcium transients evoked by Cfs that frequently occurred in close succession to the global calcium transients evoked by CSs. These local calcium transients were likely to be induced by aberrant CF branches, including transverse collaterals elongated along mediolateral axis beyond the border of cerebellar zones. In the following section, I discuss possible mechanisms for the mediolateral enhancement of synchrony in GluRδ2 KO mice by aberrant CFs.

**Origin of the mediolateral enhancement of CS synchrony in GluRδ2 KO mice**

It has been demonstrated that surplus weak CF input can induce localized calcium transients in distal dendrites of PCs in cerebellar slice preparations from GluRδ2 KO mice [36]. Morphological study also showed that ectopic CF branches in GluRδ2 KO mice innervate limited areas in the distal dendritic tree of PCs, and that transverse CF collaterals elongating in the outer molecular layer near the pial surface have

38

glutamatergic terminals around dendrites of multiple neighboring PCs [35]. These

elongated transverse CF collaterals and ectopic synapse formation occur mutually

among neighboring PCs [35]. Thus, CFs of GluRδ2 KO mice are considered to activate

their main target PCs through ascending main branches and also neighboring PCs

through transverse collaterals. Spike discharges of IO neurons in GluRδ2 KO mice can

induce global dendritic calcium transients associated with CSs in their main target PCs,

and also induce local dendritic calcium transients associated with Cfs in neighboring

PCs (Fig. 6). Furthermore, I found that Cfs tended to be induced in a rapid succession

(Fig. 3F) in close proximity to the occurrence of CS (Fig 3G). At a whole PC level,

bursts of Cfs are triggered by several aberrant branches from surrounding CFs and can

induce local calcium transients in various dendritic regions of the same PC

simultaneously. These clustered 'local' calcium signals are closely correlated in time

with the CS-evoked 'global' calcium signals observed in other neighboring PCs, and

thus significantly contribute to the enhanced synchrony in the mediolateral direction.

In contrast to the aberrant CF-PC wiring, the gap junctional coupling between

IO neurons seemed less important for the enhanced mediolateral synchrony of CF

activity in GluRδ2 KO mice (Fig. 4C, 4D). However, the synchrony between adjacent

PCs (distance between dendrites ≤ 20 µm) of GluRδ2 KO mice was reduced to the level

of wild-type mice by application of gap junction blocker (Fig. 4B). This result indicates that the gap junctional coupling among IO neurons contributes significantly to the enhanced synchrony among adjacent PCs in GluRδ2 KO mice.

**Change in firing patterns of PCs and its possible impacts on activities of the olivocerebellar loop in GluRδ2 KO mice**

I found that not only spatial pattern but also temporal pattern of CF activity was altered in GluRδ2 KO mice (Fig. 3) as reported previously [37]. This alteration in firing pattern was also important for the enhanced synchrony in mediolateral direction. Previous studies demonstrated that firing patterns of IO neurons are modulated by glutamatergic and GABAergic inputs [8, 45]. These inputs are elements of the olivocerebellar feedback loop composed of IO, PCs and deep cerebellar nuclei (DCN). IO neurons send their axons to PCs in specific cerebellar zones and collaterals to specific regions of DCN neurons that receive inhibitory inputs from the PCs with inputs from the same IO neurons. A part of DCN neurons in turn send inhibitory signals back to the IO [19, 45, 56]. On the other hand, another population of DCN neurons send excitatory inputs to mesodiencephalic nuclei, such as the red nucleus and the nucleus of Darkschewitsch, which send excitatory signals back to the IO [57]. My results suggest that these

excitatory and inhibitory inputs to the IO are likely to be altered by the change in spatial and temporal patterns of CF responses of PCs in GluRδ2 KO mice. In addition to typical CF response (CS), PCs in GluRδ2 KO mice showed a characteristic burst of action potentials (Cf), which is most likely due to surplus weak CF inputs arising from aberrant transverse CF collaterals [37]. A Cf is a burst of 2–7 full spikes at a firing rate of >180 Hz, whereas a CS consists of a single full spike followed by several smaller spikelets (Fig. 3B). As previously shown by dual somatic and axonal recordings from PCs in cerebellar slice preparations, PC axons can transmit SSs with high fidelity at >200 Hz, whereas they cannot faithfully transmit the secondary spikelets in CS [58, 59]. Therefore, weak surplus CF inputs, which induce Cfs, would have significant or even larger impact on the output of PC to DCN, compared with strong main CF inputs that induce typical CSs. Furthermore, CS and Cf in GluRδ2 KO mice fired in burst (2-16 CS/Cf at 6-12 Hz), even though the mean firing rate was not significantly different from CS firing rate of wild-type mice. Given the highly convergent nature of connections between PC and DCN neuron [60], spatial enhancement of synchrony and temporal clustering of CF activity in PCs would have striking impacts on the firings of DCN neurons in GluRδ2 KO mice. Since synchronized CSs in PCs within a microzone can induce strong hyperpolarization followed by rebound spiking in corresponding DCN

neurons [61], DCN neurons in GluRδ2 KO mice are likely to show strong rebound burst firings in response to synchronized CS/Cf clusters. Such burst firings of DCN neurons may generate burst spiking in IO neurons through the excitatory pathway involving mesodiencephalic nuclei, which may eventually be converted to CS bursts in PCs via CFs. On the other hand, burst firings of DCN neurons that send inhibitory inputs directly to the IO are thought to induce large hyperpolarization and rebound excitation in IO neurons [62, 63]. Thus, it is expected that highly synchronized PC activation by CS/Cf causes strong modulation of the firing patterns of IO neurons through rebound excitation of DCN neurons.

**Highly synchronous CF activity between PCs in GluRδ2 KO mice**

Previous studies has revealed various cytoarchitectural, electrophysiological and behavioral phenotypes of GluRδ2 KO mice, including impaired PF-PC synapse formation [31-33], persistent multiple CF innervation [32, 34, 36], deficient PF-LTD [21, 64], abnormal rhythmic CF firing [37], ataxic gait [21, 64], oscillatory eye movements [37] and impaired motor learning [21, 37, 64]. In addition to these deficits, the present study has revealed a novel phenotype of GluRδ2 KO mice that the synchrony of CF responses among neighboring PCs are greatly enhanced in the mediolateral direction of

the cerebellar cortex (Fig. 1, 2). Parasagittal longitudinal microzones based on the olivocerebellar projection are the functional units of the cerebellar cortex and play a central role in information processing in the cerebellum [5, 12]. Sensory and/or motor information can be robustly encoded in spatial patterns of activated microzones [9, 14, 65, 66], and the synchrony of CF activities among neighboring PCs in a given microzone can convey sensorimotor information without increasing the firing rates of CFs [9, 67]. In GluRδ2 KO mice, the abnormal enhancement of CF synchrony in the mediolateral direction leads to functional broadening of individual microzones and reciprocal reduction in the pattern of activated microzones. This should significantly reduce the quantity of information conveyed by CF inputs, which may result, at least in part, in motor deficits in GluRδ2 KO mice.

**Disrupted zonal organization by aberrant transverse CF collaterals in GluRδ2 KO mice**

According to the previous morphological studies, CF terminals of single IO neurons are aligned within single aldC bands, and these compartments are thought to represent functional units ("zones") for motor control of specific body parts [12]. The rate of decline in synchrony in GluRδ2 KO mice was smaller than that in wild-type mice

43

(~10 % decrease and 35-45 % decrease at 190 μm, respectively; Fig. 2B, 4D),

indicating that PCs in different zones of GluRδ2 KO mice could be activated

simultaneously. In fact, transverse CF collaterals branching from ascending CFs in an

aldC-positive band elongated into neighboring aldC-negative bands and vice versa (Fig.

5). Mean length of transverse branch was 46.9±3.0 μm (maximal length : 176.8 μm) in

GluRδ2 KO mice, but this value is likely to be underestimated and actual length would

be larger because these branches were often cut during slice preparation. Therefore,

anomalously high synchronous activation of multiple bands due to aberrant transverse

CF collaterals can spread not only over the boundary of microzones but also beyond the

border of zones, indicating that the somatotopic organization of cerebellar cortex of

GluRδ2 KO mice might be disrupted.


**Functional significance**

My findings directly demonstrate the close relationship between anatomical and

functional microzonal organization in the cerebellar cortex. Furthermore, it is possible

that aberrant transverse wiring affects the firing pattern of IO and DCN neurons through

the olivocerebellar feedback loop. During postnatal development, only one CF is

strengthened, and other surplus CFs are weakened and ultimately eliminated to establish

one-to-one relationship between CF and PC [68, 69]. Thus, functional differentiation

and elimination of redundant CFs during postnatal development are crucial to establish

the properly functional olivocerebellar loop.

**ACKNOWLEDGEMENTS**

**REFERENCES**

1.  Sugihara, I., Wu, HS and Shinoda, Y. *The entire trajectories of single olivocerebellar axons in the cerebellar cortex and their contribution to Cerebellar compartmentalization.* J Neurosci 21(19) 7715-7723. 2001

2.  Sugihara, I. *Microzonal projection and climbing fiber remodeling in single olivocerebellar axons of newborn rats at postnatal days 4-7.* J Comp Neurol 487(1) 93-106. 2005

3.  Voogd, J and Glickstein, M. *The anatomy of the cerebellum.* Trends Neurosci 21(9) 370-375. 1998

4.  Groenewegen, HJ., Voogd, J and Freedman, SL. *The parasagittal zonation within the olivocerebellar projection. II. Climbing fiber distribution in the intermediate and hemispheric parts of cat cerebellum.* J Comp Neurol 183(3) 551-601. 1979

5.  Buisseret-Delmas, C and Angaut, P. *The cerebellar olivo-corticonuclear connections in the rat.* Prog Neurobiol 40(1) 63-87. 1993

6.  Horn, KM., Pong, M and Gibson, AR. *Functional relations of cerebellar modules of the cat.* J Neurosci 30(28) 9411-9423. 2010

7.  Lang, EJ., Sugihara, I., Welsh, JP and Llinas, R. *Patterns of spontaneous purkinje cell complex spike activity in the awake rat.* J Neurosci 19(7) 2728-2739. 1999

8.  Lang, EJ. *GABAergic and glutamatergic modulation of spontaneous and motor-cortex-evoked complex spike activity.* J Neurophysiol 87(4) 1993-2008. 2002

9.  Schultz, SR., Kitamura, K., Post-Uiterweer, A., Krupic, J and Häusser, M. *Spatial Pattern Coding of Sensory Information by Climbing Fiber-Evoked Calcium Signals in Networks of Neighboring Cerebellar Purkinje Cells.* J Neurosci 29(25) 8005-8015. 2009

10. Andersson, G and Oscarsson, O. *Climbing fiber microzones in cerebellar vermis and their projection to different groups of cells in the lateral vestibular nucleus.* Exp Brain Res 32(4) 565-579. 1978

11. Apps, R and Garwicz, M. *Anatomical and physiological foundations of cerebellar information processing.* Nat Rev Neurosci 6(4) 297-311. 2005

12. Sugihara, I and Shinoda, Y. *Molecular, topographic, and functional organization of the cerebellar cortex: a study with combined aldolase C and olivocerebellar labeling.* J Neurosci 24(40) 8771-8785. 2004

13. Sugihara, I., Wu, H and Shinoda, Y. *Morphology of single olivocerebellar axons*

*labeled with biotinylated dextran amine in the rat.* J Comp Neurol 414(2) 131-148. 1999

14. Ozden, I., Sullivan, MR., Lee, HM and Wang, SSH. *Reliable Coding Emerges from Coactivation of Climbing Fibers in Microbands of Cerebellar Purkinje Neurons.* J Neurosci 29(34) 10463-10473. 2009

15. Llinas, R and Yarom, Y. *Electrophysiology of mammalian inferior olivary neurones in vitro. Different types of voltage-dependent ionic conductances.* J Physiol 315 549-567. 1981

16. Sotelo, C., Gotow, T and Wassef, M. *Localization of glutamic-acid-decarboxylase-immunoreactive axon terminals in the inferior olive of the rat, with special emphasis on anatomical relations between GABAergic synapses and dendrodendritic gap junctions.* J Comp Neurol 252(1) 32-50. 1986

17. Blenkinsop, TA and Lang, EJ. *Block of inferior olive gap junctional coupling decreases Purkinje cell complex spike synchrony and rhythmicity.* J Neurosci 26(6) 1739-1748. 2006

18. Ito, M. *The cerebellum: Brain for an Implicit Self* Ito, M. 2011

19. Chen, X., Kovalchuk, Y., Adelsberger, H., Henning, HA., Sausbier, M., Wietzorrek, G., Ruth, P., Yarom, Y and Konnerth, A. *Disruption of the olivo-cerebellar circuit by Purkinje neuron-specific ablation of BK channels.* Proc Natl Acad Sci U S A 107(27) 12323-12328. 2010

20. Kano, M., Hashimoto, K., Chen, C., Abeliovich, A., Aiba, A., Kurihara, H., Watanabe, M., Inoue, Y and Tonegawa, S. *Impaired synapse elimination during cerebellar development in PKC gamma mutant mice.* Cell 83(7) 1223-1231. 1995

21. Kashiwabuchi, N., Ikeda, K., Araki, K., Hirano, T., Shibuki, K., Takayama, C., Inoue, Y., Kutsuwada, T., Yagi, T., Kang, Y and et al. *Impairment of motor coordination, Purkinje cell synapse formation, and cerebellar long-term depression in GluR delta 2 mutant mice.* Cell 81(2) 245-252. 1995

22. Hirai, H., Pang, Z., Bao, D., Miyazaki, T., Li, L., Miura, E., Parris, J., Rong, Y., Watanabe, M., Yuzaki, M and Morgan, JI. *Cbln1 is essential for synaptic integrity and plasticity in the cerebellum.* Nat Neurosci 8(11) 1534-1541. 2005

23. Chen, C., Kano, M., Abeliovich, A., Chen, L., Bao, S., Kim, JJ., Hashimoto, K., Thompson, RF and Tonegawa, S. *Impaired motor coordination correlates with persistent multiple climbing fiber innervation in PKC gamma mutant mice.* Cell 83(7) 1233-1242. 1995

24. Kano, M., Hashimoto, K., Watanabe, M., Kurihara, H., Offermanns, S., Jiang, H.,

Wu, Y., Jun, K., Shin, HS., Inoue, Y., Simon, MI and Wu, D. *Phospholipase cbeta4 is specifically involved in climbing fiber synapse elimination in the developing cerebellum.* Proc Natl Acad Sci U S A 95(26) 15724-15729. 1998

25.    Offermanns, S., Hashimoto, K., Watanabe, M., Sun, W., Kurihara, H., Thompson, RF., Inoue, Y., Kano, M and Simon, MI. *Impaired motor coordination and persistent multiple climbing fiber innervation of cerebellar Purkinje cells in mice lacking Galphaq.* Proc Natl Acad Sci U S A 94(25) 14089-14094. 1997

26.    Landsend, AS., Amiry-Moghaddam, M., Matsubara, A., Bergersen, L., Usami, S., Wenthold, RJ and Ottersen, OP. *Differential localization of delta glutamate receptors in the rat cerebellum: coexpression with AMPA receptors in parallel fiber-spine synapses and absence from climbing fiber-spine synapses.* J Neurosci 17(2) 834-842. 1997

27.    Takayama, C., Nakagawa, S., Watanabe, M., Mishina, M and Inoue, Y. *Light- and electron-microscopic localization of the glutamate receptor channel delta 2 subunit in the mouse Purkinje cell.* Neurosci Lett 188(2) 89-92. 1995

28.    Takayama, C., Nakagawa, S., Watanabe, M., Mishina, M and Inoue, Y. *Developmental changes in expression and distribution of the glutamate receptor channel delta 2 subunit according to the Purkinje cell maturation.* Brain Res Dev Brain Res 92(2) 147-155. 1996

29.    Matsuda, K., Miura, E., Miyazaki, T., Kakegawa, W., Emi, K., Narumi, S., Fukazawa, Y., Ito-Ishida, A., Kondo, T., Shigemoto, R., Watanabe, M and Yuzaki, M. *Cbln1 is a ligand for an orphan glutamate receptor delta2, a bidirectional synapse organizer.* Science 328(5976) 363-368. 2010

30.    Uemura, T., Lee, SJ., Yasumura, M., Takeuchi, T., Yoshida, T., Ra, M., Taguchi, R., Sakimura, K and Mishina, M. *Trans-synaptic interaction of GluRdelta2 and Neurexin through Cbln1 mediates synapse formation in the cerebellum.* Cell 141(6) 1068-1079. 2010

31.    Kurihara, H., Hashimoto, K., Kano, M., Takayama, C., Sakimura, K., Mishina, M., Inoue, Y and Watanabe, M. *Impaired parallel fiber-->Purkinje cell synapse stabilization during cerebellar development of mutant mice lacking the glutamate receptor delta2 subunit.* J Neurosci 17(24) 9613-9623. 1997

32.    Ichikawa, R., Miyazaki, T., Kano, M., Hashikawa, T., Tatsumi, H., Sakimura, K., Mishina, M., Inoue, Y and Watanabe, M. *Distal extension of climbing fiber territory and multiple innervation caused by aberrant wiring to adjacent spiny branchlets in cerebellar Purkinje cells lacking glutamate receptor delta 2.* J Neurosci 22(19) 8487-8503. 2002

33.    Takeuchi, T., Miyazaki, T., Watanabe, M., Mori, H., Sakimura, K and Mishina,

M. *Control of synaptic connection by glutamate receptor delta2 in the adult cerebellum.* J Neurosci 25(8) 2146-2156. 2005

34. Miyazaki, T., Yamasaki, M., Takeuchi, T., Sakimura, K., Mishina, M and Watanabe, M. *Ablation of Glutamate Receptor GluR 2 in Adult Purkinje Cells Causes Multiple Innervation of Climbing Fibers by Inducing Aberrant Invasion to Parallel Fiber Innervation Territory.* J Neurosci 30(45) 15196-15209. 2010

35. Miyazaki, T and Watanabe, M. *Development of an anatomical technique for visualizing the mode of climbing fiber innervation in Purkinje cells and its application to mutant mice lacking GluRδ2 and Cav2.1.* Anat Sci Int 86(1) 10-18. 2010

36. Hashimoto, K., Ichikawa, R., Takechi, H., Inoue, Y., Aiba, A., Sakimura, K., Mishina, M., Hashikawa, T., Konnerth, A., Watanabe, M and Kano, M. *Roles of glutamate receptor delta 2 subunit (GluRdelta 2) and metabotropic glutamate receptor subtype 1 (mGluR1) in climbing fiber synapse elimination during postnatal cerebellar development.* J Neurosci 21(24) 9701-9712. 2001

37. Yoshida, T., Katoh, A., Ohtsuki, G., Mishina, M and Hirano, T. *Oscillating Purkinje neuron activity causing involuntary eye movement in a mutant mouse deficient in the glutamate receptor delta2 subunit.* J Neurosci 24(10) 2440-2448. 2004

38. Sullivan, MR., Nimmerjahn, A., Sarkisov, DV., Helmchen, F and Wang, SS. *In vivo calcium imaging of circuit activity in cerebellar cortex.* J Neurophysiol 94(2) 1636-1644. 2005

39. Yamasaki, M., Miyazaki, T., Azechi, H., Abe, M., Natsume, R., Hagiwara, T., Aiba, A., Mishina, M., Sakimura, K and Watanabe, M. *Glutamate Receptor  2 Is Essential for Input Pathway-Dependent Regulation of Synaptic AMPAR Contents in Cerebellar Purkinje Cells.* J Neurosci 31(9) 3362-3374. 2011

40. Mukamel, EA., Nimmerjahn, A and Schnitzer, MJ. *Automated Analysis of Cellular Signals from Large-Scale Calcium Imaging Data.* Neuron 63(6) 747-760. 2009

41. Stosiek, C., Garaschuk, O., Holthoff, K and Konnerth, A. *In vivo two-photon calcium imaging of neuronal networks.* Proc Natl Acad Sci U S A 100(12) 7319-7324. 2003

42. Denk, W., Strickler, JH and Webb, WW. *Two-photon laser scanning fluorescence microscopy.* Science 248(4951) 73-76. 1990

43. Pologruto, TA., Sabatini, BL and Svoboda, K. *ScanImage: flexible software for operating laser scanning microscopes.* Biomed Eng Online 2 13. 2003

44. Kitamura, K., Judkewitz, B., Kano, M., Denk, W and Häusser, M. *Targeted*

*patch-clamp recordings and single-cell electroporation of unlabeled neurons in vivo.* <u>Nat Methods</u> 5(1) 61-67. 2007

45. Lang, EJ., Sugihara, I and Llinas, R. *GABAergic modulation of complex spike activity by the cerebellar nucleoolivary pathway in rat.* <u>J Neurophysiol</u> 76(1) 255-275. 1996

46. Ozden, I., Lee, HM., Sullivan, MR and Wang, SSH. *Identification and Clustering of Event Patterns From In Vivo Multiphoton Optical Recordings of Neuronal Ensembles.* <u>J Neurophysiol</u> 100(1) 495-503. 2008

47. Kitamura, K and Häusser, M. *Dendritic Calcium Signaling Triggered by Spontaneous and Sensory-Evoked Climbing Fiber Input to Cerebellar Purkinje Cells In Vivo.* <u>J Neurosci</u> 31(30) 10847-10858. 2011

48. Llinas, R and Sasaki, K. *The Functional Organization of the Olivo-Cerebellar System as Examined by Multiple Purkinje Cell Recordings.* <u>Eur J Neurosci</u> 1(6) 587-602. 1989

49. Hawkes, R and Leclerc, N. *Antigenic map of the rat cerebellar cortex: the distribution of parasagittal bands as revealed by monoclonal anti-Purkinje cell antibody mabQ113.* <u>J Comp Neurol</u> 256(1) 29-41. 1987

50. Sugihara, I and Quy, PN. *Identification of aldolase C compartments in the mouse cerebellar cortex by olivocerebellar labeling.* <u>J Comp Neurol</u> 500(6) 1076-1092. 2007

51. Brochu, G., Maler, L and Hawkes, R. *Zebrin II: a polypeptide antigen expressed selectively by Purkinje cells reveals compartments in rat and fish cerebellum.* <u>J Comp Neurol</u> 291(4) 538-552. 1990

52. Voogd, J., Pardoe, J., Ruigrok, TJ and Apps, R. *The distribution of climbing and mossy fiber collateral branches from the copula pyramidis and the paramedian lobule: congruence of climbing fiber cortical zones and the pattern of zebrin banding within the rat cerebellum.* <u>J Neurosci</u> 23(11) 4645-4656. 2003

53. Voogd, J and Ruigrok, TJ. *The organization of the corticonuclear and olivocerebellar climbing fiber projections to the rat cerebellar vermis: the congruence of projection zones and the zebrin pattern.* <u>J Neurocytol</u> 33(1) 5-21. 2004

54. Pijpers, A., Voogd, J and Ruigrok, TJ. *Topography of olivo-cortico-nuclear modules in the intermediate cerebellum of the rat.* <u>J Comp Neurol</u> 492(2) 193-213. 2005

55. Sugihara, I., Marshall, SP and Lang, EJ. *Relationship of complex spike synchrony bands and climbing fiber projection determined by reference to aldolase C compartments in crus IIa of the rat cerebellar cortex.* <u>J Comp Neurol</u>

501(1) 13-29. 2007

56. de Zeeuw, CI., Holstege, JC., Ruigrok, TJ and Voogd, J. *Ultrastructural study of the GABAergic, cerebellar, and mesodiencephalic innervation of the cat medial accessory olive: anterograde tracing combined with immunocytochemistry.* J Comp Neurol 284(1) 12-35. 1989

57. De Zeeuw, CI., Simpson, JI., Hoogenraad, CC., Galjart, N., Koekkoek, SK and Ruigrok, TJ. *Microcircuitry and function of the inferior olive.* Trends Neurosci 21(9) 391-400. 1998

58. Monsivais, P., Clark, BA., Roth, A and Häusser, M. *Determinants of action potential propagation in cerebellar Purkinje cell axons.* J Neurosci 25(2) 464-472. 2005

59. Khaliq, ZM and Raman, IM. *Axonal propagation of simple and complex spikes in cerebellar Purkinje neurons.* J Neurosci 25(2) 454-463. 2005

60. Palkovits, M., Mezey, E., Hamori, J and Szentagothai, J. *Quantitative histological analysis of the cerebellar nuclei in the cat. I. Numerical data on cells and on synapses.* Exp Brain Res 28(1-2) 189-209. 1977

61. Bengtsson, F., Ekerot, C-F and Jörntell, H. *In Vivo Analysis of Inhibitory Synaptic Inputs and Rebounds in Deep Cerebellar Nuclear Neurons.* PLoS ONE 6(4) e18822. 2011

62. Choi, S., Yu, E., Kim, D., Urbano, FJ., Makarenko, V., Shin, HS and Llinas, RR. *Subthreshold membrane potential oscillations in inferior olive neurons are dynamically regulated by P/Q- and T-type calcium channels: a study in mutant mice.* J Physiol 588(16) 3031-3043. 2010

63. Khosrovani, S., Van Der Giessen, RS., De Zeeuw, CI and De Jeu, MT. *In vivo mouse inferior olive neurons exhibit heterogeneous subthreshold oscillations and spiking patterns.* Proc Natl Acad Sci U S A 104(40) 15911-15916. 2007

64. Hirai, H., Miyazaki, T., Kakegawa, W., Matsuda, S., Mishina, M., Watanabe, M and Yuzaki, M. *Rescue of abnormal phenotypes of the delta2 glutamate receptor-null mice by mutant delta2 transgenes.* EMBO Rep 6(1) 90-95. 2005

65. Welsh, JP., Lang, EJ., Suglhara, I and Llinas, R. *Dynamic organization of motor control within the olivocerebellar system.* Nature 374(6521) 453-457. 1995

66. Ghosh, KK., Burns, LD., Cocker, ED., Nimmerjahn, A., Ziv, Y., Gamal, AE and Schnitzer, MJ. *Miniaturized integration of a fluorescence microscope.* Nat Methods 8(10) 871-878. 2011

67. Welsh, JP. *Functional significance of climbing-fiber synchrony: a population coding and behavioral analysis.* Ann N Y Acad Sci 978 188-204. 2002

68. Hashimoto, K and Kano, M. *Functional differentiation of multiple climbing fiber*

*inputs during synapse elimination in the developing cerebellum.* <u>Neuron</u> 38(5) 785-796. 2003

69.    Hashimoto, K and Kano, M. *Postnatal development and synapse elimination of climbing fiber to Purkinje cell projection in the cerebellum.* <u>Neurosci Res</u> 53(3) 221-228. 2005